Applied Catalysis B: Environmental 254 (2019) 371–379

Contents lists available at ScienceDirect

Applied Catalysis B: Environmental

journal homepage: www.elsevier.com/locate/apcatb

Removal of MC-LR using the stable and efficient MIL-100/MIL-53 (Fe) photocatalyst: The effect of coordinate immobilized layers

Hailin Tian[a,b], Tirusew Araya[a,b], Ruiping Li[a,b], Yanfen Fang[b], Yingping Huang[a,b,*]

[a] College of Hydraulic & Environmental Engineering, China Three Gorges University, Yichang 443002, Hubei, China
[b] Engineering Research Center of Eco-environment in Three Gorges Reservoir Region, Ministry of Education, China Three Gorges University, Yichang 443002, Hubei, China

ARTICLE INFO

Keywords:
Fe-based MOFs
Microcystin-LR
Photodegradation

ABSTRACT

Microcystin-LR (MC-LR), which is produced from cyanobacteria, is the common microcystin with a serious threat to aquatic life and human beings. And the efficient removal method of MC-LR is urgent needed. In this work, the MIL-100/MIL-53 (Fe) photocatalysts, which were successfully prepared by the electrostatic interaction with each other, were applied for the photocatalytic degradation of MC-LR. The structure and optical properties of the MIL-100/MIL-53 (Fe) photocatalysts were characterized by using SEM, XRD, XPS, FT-IR and UV–vis DRS. The very low dosage of the MIL-100/MIL-53 (Fe) photocatalysts achieved the degradation of MC-LR, and the optimized loading was the 50% MIL-100/MIL-53 (Fe) photocatalyst. Compared to MIL-100 (Fe) and MIL-53 (Fe), the MC-LR degradation was up to 96.5% after 3 h under visible light illumination with the 50% MIL-100/MIL-53 (Fe) photocatalyst due to the pore-effect adsorption and the effective separation of photogenerated carriers. The effect of coordinate immobilized layers between MIL-100 (Fe) and MIL-53 (Fe) contributed to the stable and efficient removal of MC-LR for the 50% MIL-100/MIL-53 (Fe) photocatalyst. The MC-LR photocatalytic mechanism and degradation pathway, which the photogenerated holes (h^+) were the main active species, were proposed by radical capture experiments and LC-MS analysis.

1. Introduction

Microcystins (MCs) are the well-known cyclic heptapeptide toxins. The toxigenic cyanobacterial blooms produced a large amount of MCs in eutrophic water, which has attracted more and more concerns in environmental safety [1]. So far, there are over 90 variants of MCs, Microcystin-LR (MC-LR), which is a strongly liver tumor promoter and protein phosphatase inhibitor, is mostly found in different water bodies among MCs [2]. The provisional value for MC-LR in drinking water criteria is 1 μg/L by the World Health Organization (WHO) [3]. Adsorption and biodegradation are the effective methods for the elimination of organic pollutants [4,5]. However, the removal of MC-LR from potable water is still a challenging task because MCs cyclic structure is stable even under a high temperature and UV irradiation [6]. In recent years, advanced oxidation technologies (AOTs), such as photocatalytic method [7], Fenton or Photo-Fenton techniques [8], and photochemical method [9], are proved to be promising techniques for the removal of MC-LR. The photocatalytic degradation of MC-LR has been widely investigated due to high efficiency, low energy consumption and eco-friendly [10,11]. And the development of photocatalysts is a key to enhance the removal efficiency of MC-LR in aqueous solutions.

Metal organic frameworks (MOFs), which are consisted of a porous three-dimensional structure between metal ions and organic linkers, have received increasing attentions in the potential of the chemical industry [12,13]. Fe-based MOFs are a promising photocatalytic material of visible light response due to the existence of extensive iron oxo clusters [14]. The photocatalytic activity of Fe-based MOFs have been developed rapidly for the degradation of pollutants in environment [15,16]. MIL-53 (Fe), where MIL stands for Materials from Institute Lavoisier, is the flexible solid with corner-sharing chains of $FeO_4(OH)_2$ octahedral connected through terephthalate moieties [17]. MIL-53 (Fe) can be used for the photocatalytic reduction of Cr (VI) and the photocatalytic degradation of organic pollutants as a potential material in environmental restoration [18,19]. However, the photocatalytic activity of MIL-53 (Fe) will be affected by the fast recombination of photogenerated electrons and holes. And iron contamination problems are usually ignored in the photocatalytic process due to the dissolution of the MIL-53 (Fe) framework.

Among various kinds of methods, the formation of MOFs composites is one of the most effective methods to improve the structural stability and photocatalytic activity. Resin/MIL-53 (Fe) [20], TiO_2@NH_2-MIL-125 (Ti) [21] and MOFs@rGO [22] are responsible for the efficient

* Corresponding author at: College of Hydraulic & Environmental Engineering, China Three Gorges University, Yichang 443002, Hubei, China.
E-mail address: chem_ctgu@126.com (Y. Huang).

https://doi.org/10.1016/j.apcatb.2019.04.086
Received 28 December 2018; Received in revised form 21 April 2019; Accepted 23 April 2019
Available online 27 April 2019

separation of electron-hole pairs, and thereby enhances the photocatalytic activity compared to the pristine MOFs. Additionally, as the bi-MOFs type photocatalysts, the UiO-66-NH_2@MIL-101 (Fe) exhibited the excellent activity for the styrene oxidation due to a well-matched band gap structure and a remarkable photoexcited carrier separation [23]. The MIL-100 (Fe) framework, which the organic linker is 1,3,5-benzene tricarboxylic acid, also contains iron (III) oxide clusters as the absorption antennae of visible light and active sites for the photocatalytic reaction. The report indicated that the MIL-100(Fe)@MIL-53 (Fe) photocatalyst in the degradation of MO achieved 100% at 80 min in the presence of 150 μL H_2O_2 and air bubbling [24]. It is demonstrated that the strategy based on two types of MOFs as the hybrid photocatalysts is a new and promising method to improve the photocatalytic efficiency. The main advantage of MIL-100/MIL-53 (Fe) composites is the formation of coordinate immobilized layers due to the coordination with unsaturated metal sites, which can contribute to the stable and tight interfacial contact between MIL-100 (Fe) and MIL-53 (Fe). Moreover, MOFs have exhibited the attractive prospects to removal micropollutants in the environment. MIL-100 (Al) gels [25] and MOFs-101 (Cr)-Py [26] have been reported as powerful adsorbents to remove MC-LR molecules. MOFs-101 (Cr)-Py reveals the remarkable performance to the adsorption of MC-LR when the dosage of adsorbent is just 0.005 g/L. Up to now, the reports on the photodegradation MC-LR and the photocatalytic mechanism by using the MOFs photocatalyst are rather scarce. Thus, it is a promising material to remove MC-LR and to systematically analysis the photocatalytic mechanism with the MIL-100/MIL-53 (Fe) photocatalyst.

Herein, we were successfully prepared the stable and efficient MIL-100/MIL-53 (Fe) photocatalyst by a simple electrostatic interaction way for the degradation of MC-LR. MIL-100 (Fe) was defined as the main active site and loaded on MIL-53 (Fe) which was used as the light harvesting materials. Compared to MIL-100 (Fe) and MIL-53 (Fe), the MC-LR photodegradation of the 50% MIL-100/MIL-53 (Fe) photocatalyst achieved 96.5% with the low dosage of 0.02 g/L under visible light irradiation for 3 h due to the pore-effect adsorption and the effective separation of photogenerated carriers. The stable and efficient removal of MC-LR for the 50% MIL-100/MIL-53 (Fe) photocatalyst was attributed to the effect of coordinate immobilized layers between MIL-100 (Fe) and MIL-53 (Fe). The MC-LR photocatalytic mechanism and degradation pathway, which photogenerated holes (h^+) was directly oxidation to form different intermediate products, were proposed by radical capture experiments and LC-MS analysis in the photocatalytic process. It is demonstrated that the 50% MIL-100/MIL-53 (Fe) photocatalyst was a fascinating material for the removal of MC-LR.

2. Experimental

2.1. Chemicals and reagents

All reagents and solvents were used as received from commercial suppliers without further purification. Iron (III) chloride hexahydrate ($FeCl_3{\cdot}6H_2O$), iron powder (400 mesh), hydrochloric acid (38%), nitric acid (65%), hydrofluoric acid (40%), sodium hydroxide (NaOH) and ammonium oxalate (AO) were supported by Sinopharm Chemical Reagent. 1,3,5-benzene tricarboxylic acid (H_3BTC), 1,4-benzene dicarboxylic acid (H_2BDC), N,*N*-dimethylformamide (DMF) and trifluoroacetic acid (TFA) were purchased from Aladdin Reagent. Microcystin-LR (MC-LR, 1 mg) was obtained from Express Technology. The MC-LR stock solution (1000 mg/L) was prepared by dissolving MC-LR in 1 mL ultrapure water. High-performance liquid chromatography (HPLC) methanol was supplied by J.T. Baker. Deionized water was purified by ShenYuan instrument with reverse osmosis membrane. 0.1 M HCl and 0.1 M NaOH were used to adjust the pH of aqueous solutions. The environment water samples were obtained from Xiangxi River in Hubei province of China.

2.2. Preparation of photocatalysts

MIL-100 (Fe) was prepared by a reported method [27]. In a typical process, a hydrothermal reaction mixture with mole ratio 1.0 Fe°: 0.66 H_3BTC: 2.0 HF: 1.2 HNO_3: 280 H_2O was loaded into a Teflon autoclave and then heated at 150 °C for 12 h to synthesize MIL-100 (Fe). The as-synthesized MIL-100 (Fe) was further purified using boiling water at 80 °C for 5 h and followed with hot ethanol at 60 °C for 3 h in order to remove the residual H_3BTC. Finally, the solid was dried under vacuum overnight at 60 °C.

MIL-53 (Fe) was synthesized by the solvothermal method according to Liang et al. [18]. Briefly, a mixture of $FeCl_3{\cdot}6H_2O$ (2.02 g, 5 mmol), H_2BDC (0.83 g, 5 mmol) and 100 mL DMF was transferred to a Teflon autoclave which was heated at 150 °C for 15 h. After cooling, the suspension was centrifuged and washed with deionized water. To remove the occluded DMF, the solid was heated at 150 °C for 12 h and stirred overnight in 200 ml anhydrous methanol.

The as-prepared MIL-53 (Fe) (0.5 g) was dispersed in 100 mL deionized water under the ultrasound condition. The MIL-53 (Fe) suspension and certain amount of MIL-100 (Fe) were stirred at room temperature for 48 h. The supernatant was removed by filtration and the residual product was washed by deionized water for 3 times, and then dried at 60 °C for 8 h. The MIL-100/MIL-53 (Fe) photocatalysts can be obtained in various proportions of the MIL-100 (Fe) weight (1%, 5%, 50%).

2.3. Characterization of photocatalysts

The morphology of different photocatalysts was observed by using a JSM-7500 F (JEOL, Japan) scanning electron microscope (SEM). XRD patterns were obtained on an Ultima IV X-ray diffractometer (Rigaku, Japan) operated at 40 kV with Cu Kα irradiation (λ = 0.15406 nm). The data were recorded in the 2θ range of 5–50°. UV–vis diffuse reflectance spectra (UV–vis DRS) were investigated by a UV-3100 spectrophotometer (Shimadzu, Japan) with $BaSO_4$ as a reflectance standard. X-ray photoelectron spectroscopy (XPS) measurements were conducted on a Multilab 2000 XPS system (VG, USA) with a monochromatic Al Kα X-ray source. FT-infrared (FT-IR) spectra were carried out on a Nicolet 6700 FT-IR spectrometer (Thermo, USA). The Photoluminescence (PL) measurements were performed by a fluorescence spectrophotometer (Hitachi, Japan) using a Xenon lamp as the excitation source with an excitation wavelength of 290 nm. Zeta potentials of different samples in the aqueous solution were obtained by using a zeta potential instrument (Malvern, UK).

2.4. Photocatalytic degradation and intermediate products analysis of MC-LR

In the photodegradation experiment, 2 mg of the as-prepared photocatalysts was dispersed in 20 mL of deionized water with ultrasound to obtain a homogenous suspension. 2 mL of the homogeneous suspension and 8 ml of deionized water were added in a 20 mL test tube. Then, 45 μL of the MC-LR stock solution with 1000 mg/L was injected into the tube to form 4.5 mg/L MC-LR solution. The solution (pH = 7) was adjusted by 0.1 M NaOH. The degradation of MC-LR under visible light irradiation was examined at room temperature in air with a XPA-7 photocatalytic reactor (Xujiang, China). The reaction tubes were irradiated by a 400 W Xe lamp with a 420 nm cutoff filter. The distance between the light source and reaction tubes was fixed at 10 cm [20]. The suspension was magnetically stirred in the dark for 90 min to ensure the adsorption/desorption equilibrium. The reactive solution of 400 μL was withdrawn at regular time interval and centrifuged at 10,000 rpm for 25 min to prepare the sample for HPLC analysis.

HPLC analysis was performed by using Waters 600 with a 2998 photodiode array (PDA) detector and a C_{18} reverse-phase column (4.6 mm × 250 mm, Kromasil). The flow rate, injection volume,

column temperature and detection wavelength were 0.8 mL/min, 20 μL, 35 °C and 238 nm, respectively. The mobile phase was consisted of 60% methanol and 40% water contained 0.05% TFA. LC-MS analysis was employed by Agilent LC/MSD Trap1100 to analyze reaction intermediates by fully scanning from m/z 200 to 1150 in the positive ion mode.

2.5. Stability and recyclability of photocatalysts

The stability of different photocatalysts was evaluated by measuring the Fe ions leaching during the photocatalytic process. 500 μL of hydroxylamine hydrochloride (0.1 g/mL) was added into the suspension of MIL-100 (Fe), MIL-53 (Fe) and the 50% MIL-100/MIL-53 (Fe) photocatalyst (5 mg/mL), respectively. And then 100 μL of 1,10-phenanthroline monohydrate (1.5 mg/mL) was added into the above mixing solution. The absorbance of the mixing solution was measured at 510 nm [28]. The recyclability of the 50% MIL-100/MIL-53 (Fe) photocatalyst was evaluated by cycling tests for the degradation of MC-LR. 1 mg the photocatalyst was dispersed into 50 mL MC-LR (4.5 mg/L) and the solution (pH = 7) was adjusted by 0.1 M NaOH. After each photocatalytic cycling experiment, the aqueous suspension from the residual and withdrawn samples was collected. The photocatalyst was separated by a centrifugation process and washed 3 times with ethanol and deionized water in ultrasound to completely remove the absorbed MC-LR and byproducts on the surface of the 50% MIL-100/MIL-53 (Fe) photocatalyst. Then the photocatalyst was centrifuged at 10,000 rpm for 25 min and dried in vacuum at 150 °C for 4 h.

2.6. Electrochemical analysis

The electrochemical measurements were performed by CHI66E electrochemical workstation (Chenhua, China) with a conventional three-electrode cell system. A Pt electrode was used as the counter electrode, an Ag/AgCl electrode (Satd, KCl) as the reference electrode and as-prepared photocatalysts on FTO glass as the working electrode. The working electrode was prepared as follows: 10 mg of the photocatalysts was ultrasonically dispersed in 0.1 mL ethanol and 2 μL Nafion solutions (wt. 5%). Then, 25 μL of slurry was dropped on the FTO glass surface (area of 1 × 1 cm) and placed in a vacuum oven at 60 °C for 12 h. The Mott-Schottky analysis (frequency of 1 kHz) was performed in 0.5 M Na_2SO_4 as the electrolyte solution.

3. Results and discussion

3.1. Morphology, structure and elemental analysis of photocatalysts

The morphology and crystal structure of different photocatalysts are characterized by using SEM and XRD in Fig. 1. As shown in Fig. 1A, the morphology of MIL-53 (Fe) shows a well crystallized rod-like structure, and the diameter of the rod-like MIL-53 (Fe) is about 5–10 μm in supplemental materials (Fig. S1A). The original MIL-100 (Fe) displays the particle-like morphology with different sizes ranging from 0.1 to 1 μm in Fig. 1B [27]. SEM image of the 50% MIL-100/MIL-53 (Fe) photocatalysts can be seen in Fig. 1C, while MIL-100 (Fe) particles are dispersed on the surface of MIL-53 (Fe) as the support (Fig. S1B). SEM-EDS linear scanning results of the 50% MIL-100/MIL-53 (Fe) photocatalyst were presented in Fig. S1C. The C content is higher at the center, while the Fe and O content have no apparent change at the overall line. This reason can be explained by different C contents of the organic linker in MIL-100 (Fe) and MIL-53 (Fe). SEM-EDS linear scanning results indicated that MIL-100 (Fe) particles were anchored on the surface of MIL-53 (Fe) probably by immobilized layers. As shown in Fig. 1D, XRD patterns of the as-synthesized MIL-100 (Fe) and MIL-53 (Fe) reveals the formation of the crystallized MOFs structure. The characteristic peaks of MIL-100 (Fe) can be observed in the 50% MIL-100/MIL-53 (Fe) photocatalyst. And no diffraction peaks from impurities can be detected. The results indicated that the MIL-100/MIL-53 (Fe) photocatalysts were successfully prepared.

The surface chemical state of different elements in as-prepared photocatalysts was investigated by using XPS measurements. High resolution XPS spectra of C 1s in the 50% MIL-100/MIL-53 (Fe) photocatalysts are represented in Fig. 2A, and two main peaks at 284.7 eV and 288.7 eV are contributed to the sp^2-bonded carbon inside the aromatic structure and carboxylate groups of organic linkers, respectively [18]. As shown in Fig. 2B, the peak at 531.6 eV belongs to the carboxylic oxygen atoms of H_3BTC and H_2BDC in the 50% MIL-100/MIL-53 (Fe) photocatalysts. Fig. 2C shows the high resolution spectra of Fe 2p in different photocatalysts can be deconvoluted into two peaks, which belongs to Fe $2p_{3/2}$ and Fe $2p_{1/2}$, respectively. Compared to MIL-100 (Fe) and MIL-53 (Fe), the Fe 2p peaks of the 50% MIL-100/MIL-53 (Fe) photocatalyst in Fig. 2D shift 0.2–0.3 eV to the intervening binding energy at 711.6 eV and 725.3 eV, which means an intimate interfacial contact has been constructed between MIL-100 (Fe) and MIL-53 (Fe) [29]. It is demonstrated that coordinate immobilized layers has been formed in the 50% MIL-100/MIL-53 (Fe) photocatalysts, which is consistent with the result of SEM-EDS.

FT-IR spectra of MIL-100 (Fe), MIL-53 (Fe) and the MIL-100/MIL-53 (Fe) photocatalysts are presented in Fig. 3. The broad peak centered at 3500 cm^{-1} in the spectrum is attributed to the result of O—H stretching in the hydroxyl. The infrared absorption spectrum of MIL-53 (Fe) is consistent with the reported data in the literature [18]. The fingerprint area, between 1500 and 1000 cm^{-1} shows various peaks which have been assigned to the vibrations of organic ligands in the framework of MOFs. The binding energy peaks at 746 cm^{-1} and 622 cm^{-1} correspond to C–H bonding vibrations of the benzene ring and the formation of a Fe-oxo bond between the carboxylic group and Fe (III) ions, respectively [30]. The peaks between 1700 and 1300 cm^{-1} are related to the carboxylate ligand, which are attributed to the coordination of terephthalic acid and trimesic acid to the iron sites. The sharp peak of MIL-100 (Fe) at 1640 can be assigned to C═O vibrations of carboxyl groups. And the two peaks at 1530 cm^{-1} and 1390 cm^{-1} are attributed to asymmetric and symmetric vibrations of carboxyl groups, respectively [31]. These peaks of MIL-100 (Fe) and MIL-53 (Fe) are also observed in the MIL-100/MIL-53 (Fe) photocatalysts. Therefore, the FT-IR spectra confirmed the formation of MIL-100 (Fe), MIL-53(Fe) and the MIL-100/MIL-53 (Fe) photocatalysts.

3.2. Optical properties and MC-LR photodegradation of photocatalysts

The optical absorption of MIL-100 (Fe), MIL-53 (Fe) and the MIL-100/MIL-53 (Fe) photocatalysts was investigated by UV–vis DRS. As shown in Fig. 4A, MIL-100 (Fe), MIL-53 (Fe) and the MIL-100/MIL-53 (Fe) photocatalysts reveal the visible light harvesting ability. The 50% MIL-100/MIL-53 (Fe) photocatalyst displays the higher and broader adsorption spectrum than that of MIL-100 (Fe) and MIL-53 (Fe), indicating that the MIL-53 (Fe) support improves the optical activity of MIL-100 (Fe). The band gap of different photocatalysts can be calculated from a plot of transformed Kubelka-Munk function versus the energy of absorbed light [32]. Fig. 4B shows the optical band gap of the MIL-53 (Fe) and 50% MIL-100/MIL-53 (Fe) photocatalyst is around 2.73 eV for both, while the band gap of MIL-100 (Fe) is 2.6 eV. In Fig. 4C, the flat band potential of MIL-53 (Fe) and MIL-100 (Fe) determined from the Mott-Schottky plot is ca. −0.44 eV and −0.52 eV vs. Ag/AgCl, corresponding to −0.24 eV and −0.32 eV vs. NHE, respectively. The valence band (E_{VB}) can be calculated from the empirical equation $E_g = E_{VB} - E_{CB}$, where E_g is the band gap energy of the semiconductor and the conduction band (E_{CB}) is close to the flat band potential [18]. Correspondingly, the valence band (E_{VB}) of MIL-53 (Fe) and MIL-100 (Fe) is 2.49 eV and 2.28 eV, respectively. Therefore, in the 50% MIL-100/MIL-53 (Fe) photocatalyst, the photogenerated electrons will be migrated on the conduction band of MIL-53 (Fe), and the photogenerated holes are injected into the valence band of MIL-100 (Fe),

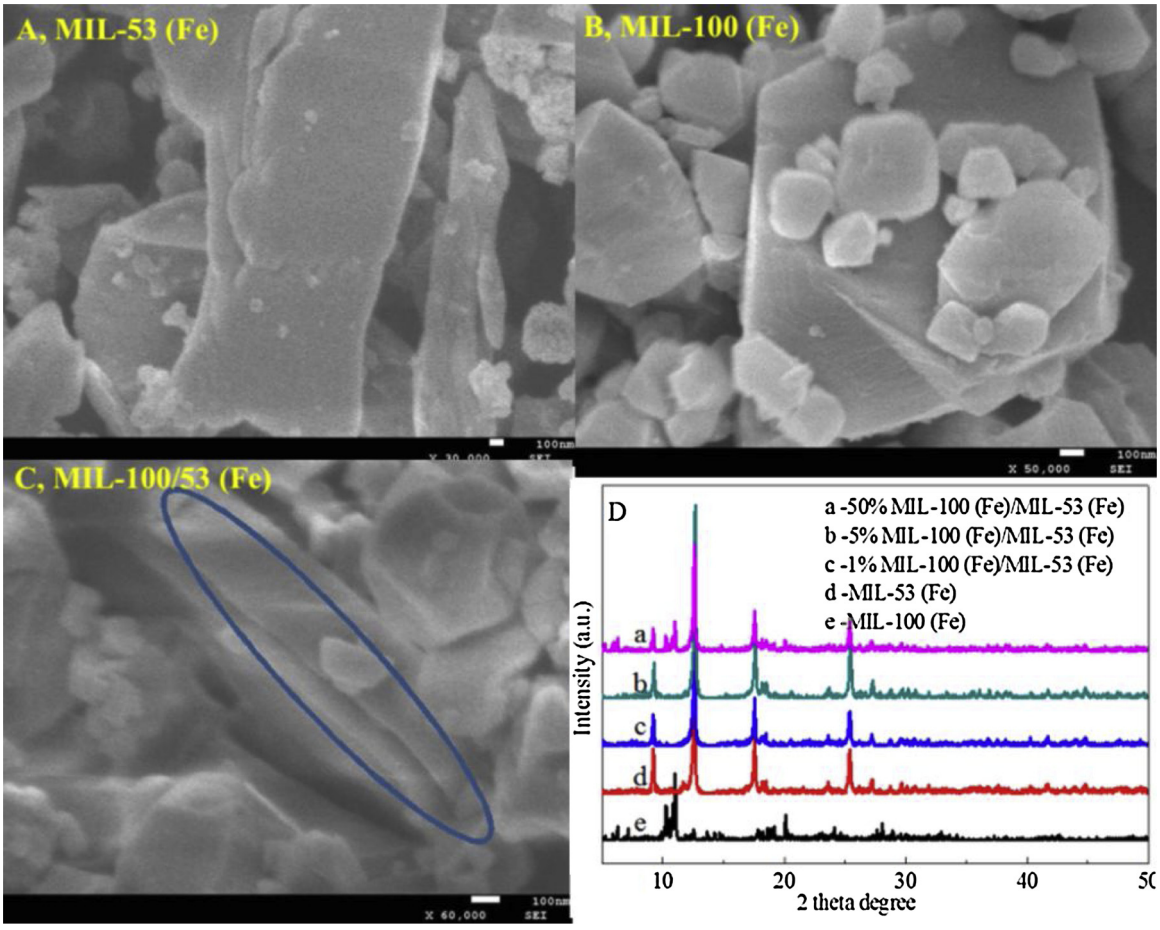

Fig. 1. SEM images of (A) MIL-53 (Fe), (B) MIL-100 (Fe), and (C) the 50% MIL-100/MIL-53 (Fe) photocatalyst, (D) XRD patterns of MIL-100 (Fe), MIL-53 (Fe) and the MIL-100/MIL-53 (Fe) photocatalysts with different loadings.

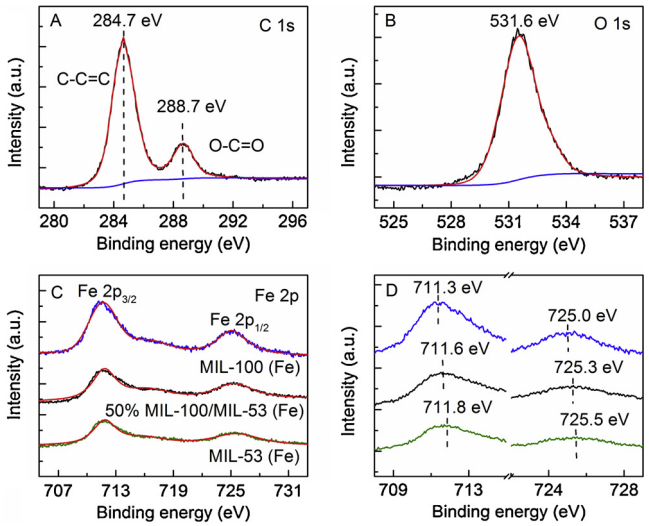

Fig. 2. (A) XPS high-resolution spectrum of C 1s and (B) O 1s in the 50% MIL-100/MIL-53 (Fe) photocatalyst, (C) XPS high-resolution spectra of Fe 2p and (D) the shifting binding energy of Fe $2p_{3/2}$ and Fe $2p_{1/2}$ in MIL-100 (Fe), MIL-53 (Fe) and the 50% MIL-100/MIL-53 (Fe) photocatalyst.

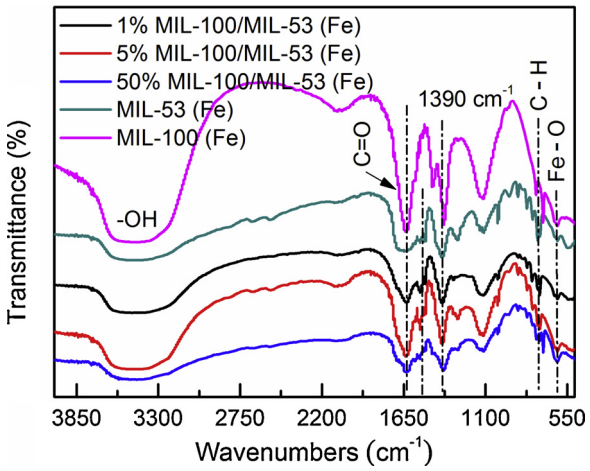

Fig. 3. FT-IR spectra of bare MIL-100 (Fe), MIL-53 (Fe) and the MIL-100/MIL-53 (Fe) photocatalysts with different loadings.

resulting the effective separation of photogenerated electron-hole pairs. Moreover, the recombination rate of photogenerated carriers was further investigated by (PL) spectra. As shown in Fig. 4D, the room-temperature PL spectra of MIL-100 (Fe), MIL-53 (Fe) and the 50% MIL-100/MIL-53 (Fe) photocatalyst were measured at the excitation wavelength of 290 nm. Obviously, the longer lifetime of photogenerated carriers in the 50% MIL-100/MIL-53 (Fe) photocatalysts can be observed as the PL peak intensity is weaker than bare MOFs [24].

Photocatalytic degradation of MC-LR under visible light irradiation was carried out to investigate the superiority of the MIL-100/MIL-53 (Fe) photocatalysts. As shown in Fig. 5A, compared to MIL-100 (Fe) and MIL-53 (Fe), the 50% MIL-100/MIL-53 (Fe) photocatalyst shows the best removal efficiency of MC-LR. The apparent rate constants and cycling stability experiments for the 50% MIL-100/MIL-53 (Fe)

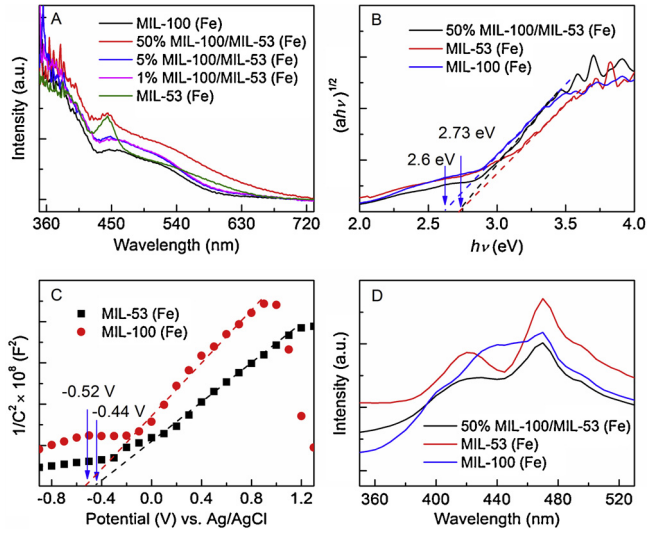

Fig. 4. (A) UV–vis DRS of different photocatalysts, (B) Optical band gap obtained from the plots of $(\alpha h\nu)^{1/2}$ versus the photon energy, (C) Typical Mott-Schottky plots in 0.5 M Na_2SO_4 aqueous solution and (D) PL spectra of MIL-100 (Fe), MIL-53 (Fe) and the 50% MIL-100/MIL-53 (Fe) photocatalyst.

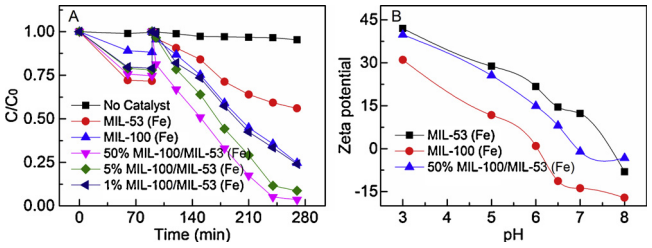

Fig. 5. (A) Photodegradation of MC-LR under visible light irradiation with bare MIL-53 (Fe), MIL-100 (Fe) and the MIL-100/MIL-53 (Fe) photocatalysts [photocatalyst dosage] = 0.02 g/L, [MC-LR] = 4.5 mg/L, pH = 7, (B) Zeta potential of MIL-53 (Fe), MIL-100 (Fe) and the 50% MIL-100/MIL-53 (Fe) photocatalyst as a function of pH.

photocatalyst and the 5% MIL-100/MIL-53 (Fe) photocatalyst are presented in the supplemental materials (Fig. S2). The apparent rate constants were estimated to be 0.0184 min^{-1}, 0.0138 min^{-1} for the 50% MIL-100/MIL-53 (Fe) and 5% MIL-100/MIL-53 (Fe) photocatalyst, respectively. Besides, the 50% MIL-100/MIL-53 (Fe) photocatalyst is more stable for the degradation of MC-LR than that of 5% one. Generally, the photocatalytic degradation mainly depends on the adsorption activity for the used photocatalyst. As can be seen from Fig. 5B, the zeta potential of MIL-53 (Fe) shows the positive potential, while MIL-100 (Fe) is the negative surface at pH 7. The 50% MIL-100/MIL-53 (Fe) photocatalyst shows a point of zero charge in neutral pH, indicating that the adsorption of MC-LR is not contributed with the electrostatic attraction. The BDC ligands point in four directions to form one-dimensional lozenge-shaped pores (0.85 nm) and aromatic ring walls in MIL-53 (Fe) [33]. The pore structure of MIL-100 (Fe) delimits two types of mesoporous cages with internal free diameters of 2.5 nm and 2.9 nm. And the smaller cages exhibit pentagonal windows with a free opening of 1.2 nm, while the larger cages possess both pentagonal and hexagonal windows with a 1.5 nm and 1.6 nm free apertures, respectively. The molecular size of MC-LR can be known in the reference (1.9 nm × 1.1 nm × 1.5 nm) [34]. Obviously, MC-LR molecule cannot completely enter the pore of both MIL-53 (Fe) and MIL-100 (Fe) because the pore windows are smaller than the size of MC-LR. However, MC-LR molecule can partially enter the pore of the 50% MIL-100/MIL-53 (Fe) photocatalyst as the pore window is large enough for the carboxyl (−COOH) and phenyl groups (-C_6H_5) [27]. Besides, the π-π interaction of benzene rings between MC-LR and organic linkers [35] may also contribute to the adsorption of MC-LR in the 50% MIL-100/MIL-53 (Fe) photocatalyst. Therefore, the pore-effect adsorption can explain the enhanced removal of MC-LR in the 50% MIL-100/MIL-53 (Fe) photocatalyst even at neutral pH.

The comparison of different heterogeneous photocatalysts for MC-LR degradation is given in Table 1. Evidently, the MIL-100/MIL-53 (Fe) photocatalyst exhibited an excellent degradation activity of MC-LR, even at the very low photocatalyst dosage. The huge surface area and pore structure of MOFs can be effectively adsorbed MC-LR molecules in the solution [26], which is significantly contributed to the degradation of MC-LR. Additionally, the removal of MC-LR with the MIL-100/MIL-53 (Fe) photocatalyst can be accomplished at neutral pH. The advantage of low photocatalyst dosage and neutral pH for the MIL-100/MIL-53 (Fe) photocatalyst is favorable to the reduction of iron contamination problems, suggesting that it has a potential in real water and wastewater treatment.

To investigate the effect of pH for the degradation of MC-LR, the experiment was carried out at different pH (3, 5, 7, 9) with the 50% MIL-100/MIL-53 (Fe) photocatalyst. The p*K*a values of MC-LR are 2.09, 2.19 and 12.48 with the ionization of two carboxylic groups and one free amino group, and MC-LR is negatively charged in the range of pH 3–9 [6]. Based on the result of Fig. 5B, the 50% MIL-100/MIL-53 (Fe) photocatalyst is positively charged at the acidic pH (3 and 5), while the photocatalyst is negative surface at pH greater than 7. Accordingly, as shown in Fig. 6A, the adsorbed MC-LR of the 50% MIL-100/MIL-53 (Fe) photocatalyst is inversely proportional to the initial pH of the solution. However, the 50% MIL-100/MIL-53 (Fe) photocatalyst shows the highest removal of MC-LR at the neutral pH 7 under the visible light irradiation. The heterostructure of the 50% MIL-100/MIL-53 (Fe) photocatalyst is unstable at pH 3 and 5, which may be the main reason for the lower photocatalytic activity. At pH 9, the photodegradation of MC-LR is restricted because the photocatalyst and MC-LR will repulse with each other. Therefore, the neutral pH 7 can be applied to an appropriate condition in the photodegradation of MC-LR for the 50% MIL-100/MIL-53 (Fe) photocatalyst. Besides, the effect of components of water on the MC-LR removal has been evaluated with the 50% MIL-100/MIL-53 (Fe) photocatalyst. Fig. 6B illustrates that the MC-LR removal of the 50% MIL-100/MIL-53 (Fe) photocatalyst is decreased about 24% and 58.5% in tap water and river water. The following reasons can be explained to the decreased degradation rate of MC-LR. The active sites of the 50% MIL-100/MIL-53 (Fe) photocatalyst are occupied by ions and the active species can be consumed by natural organic matter and minerals in environmental water [38].

Table 1
Comparison of different heterogeneous photocatalysts for MC-LR degradation.

Photocatalysts	Catalyst dosage	Initial MC-LR concentration	pH	Irradiation time	Removal ratio	Refs.
α-Fe_2O_3/γ-Fe_2O_3	0.5 g/L	0.5 mg/L	5.8	5 h	86%	[2]
N-TiO_2/$NiFe_2O_4$	1.0 g/L	0.45 mg/L	5.7	5 h	100%	[36]
Ag_3PO_4/NG/PI	0.5 g/L	5 mg/L	-[a]	10 h	94.4%	[7]
BiOBr	0.2 g/L	3 mg/L	-[a]	5 h	96.3%	[37]
MIL-100/MIL-53 (Fe)	0.02 g/L	4.5 mg/L	7	3 h	96.5%	This work

[a] The solution pH was not given.

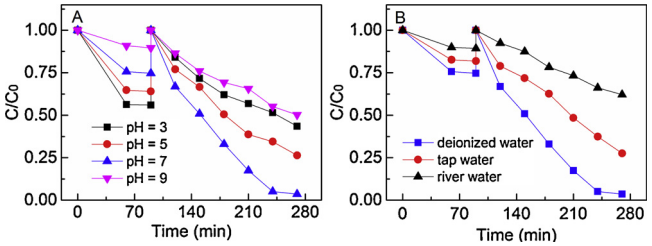

Fig. 6. (A) Photodegradation of MC-LR under different pH with the 50% MIL-100/MIL-53 (Fe) photocatalyst [photocatalyst dosage] = 0.02 g/L, [MC-LR] = 4.5 mg/L, (B) Effect of water matrix on the MC-LR removal with the 50% MIL-100/MIL-53 (Fe) photocatalyst [photocatalyst dosage] = 0.02 g/L, [MC-LR] = 4.5 mg/L, pH = 7.

3.3. MC-LR photocatalytic active species and degradation intermediates

The radical trapping experiment was performed to show the specific role of the different active species during the oxidative degradation of MC-LR, by adding various probing agents in the photodegradation system. Specifically, isopropanol, ammonium oxalate and p-benzoquinone were employed as ·OH scavenger, h^+ scavenger and $\cdot O_2^-$ scavenger, respectively. As shown in Fig. 7, compared to the system without any scavenger, the degradation of MC-LR is decreased by 56.4% after adding ammonium oxalate (h^+ scavenger) and decreased by 17.3% after adding p-benzoquinone ($\cdot O_2^-$ scavenger) on the 50% MIL-100/MIL-53 (Fe) photocatalyst. However, there is an insignificant inhibition when isopropanol (·OH scavenger) was added in the solution. It is demonstrated that photogenerated holes (h^+) is the main active species and $\cdot O_2^-$ is just a small contribution to the photodegradation of MC-LR, whereas ·OH plays little role in the degradation.

For the photodegradation mechanism of MC-LR by the MIL-100/MIL-53 (Fe) photocatalyst, the primary products were analyzed by LC-MS data. Several primary oxidative products were identified, which shows that the oxidative degradation reaction does occur (Table 2), instead of a simple adsorption or hydrolysis of MC-LR. The radical trapping experiment indicated that photogenerated holes (h^+) are the main active species. According to the detected products and intermediates, the photodegradation pathway of MC-LR by the MIL-100/MIL-53 (Fe) photocatalyst was proposed in Fig. 8. Briefly, three di-hydroxylated products (m/z 1029.7) of Adda dienes in MC-LR are generated by the photocatalytic oxidation of the 50% MIL-100/MIL-53 (Fe) photocatalyst [39]. Subsequently, it can be observed that the cleavage of the Adda chain generates the ketone-derivative at m/z 835.5 [9]. The aldehyde product (m/z 795.4) derived from the hydrolysis of the

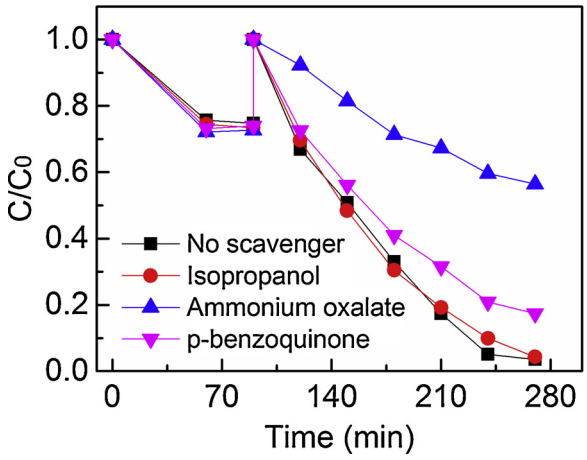

Fig. 7. Radical trapping experiments with the 50% MIL-100/MIL-53 (Fe) photocatalyst in the removal of MC-LR [photocatalyst dosage] = 0.02 g/L, [MC-LR] = 4.5 mg/L, pH = 7.

Table 2
MC-LR degradation intermediates with the 50% MIL-100/MIL-53 (Fe) photocatalyst by LC-MS analysis.

m/z $[M+H]^+$	RT (min)	Chemical formula
995.5	32.4–32.8	$C_{49}H_{74}N_{10}O_{12}$
1029.7	27–28	$C_{49}H_{76}N_{10}O_{14}$
835.5	50–52	$C_{37}H_{58}N_{10}O_{12}$
795.4	45–47	$C_{34}H_{54}N_{10}O_{12}$
783.4	47.5–48.5	$C_{33}H_{50}N_8O_{14}$

dihydroxylation product on the Adda chain can also be detected in the LC-MS data. Due to direct photo-induced holes oxidation followed by hydrolysis, the nitro-contained product (m/z 783.4) is formed during the guanidine group oxidation [37]. Although the destruction of MC-LR peptide bonds is not observed, the toxicity of MC-LR can be alleviated by the cleavage of the diene bond in the Adda chain [40].

3.4. Stability and recyclability of photocatalysts

Stability is one of the most important parameter when the photocatalyst is used for the removal of pollutants. Leaching of iron ion from Fe-based MOFs is the main reason for metal contamination problems [41]. As can be seen from Fig. 9A, the iron leakage has decreased significantly in the 50% MIL-100/MIL-53 (Fe) photocatalyst, and this result is also proved form the color of the aqueous solution (Inset of Fig. 9A) during the photocatalytic process. Additionally, the magnetic property of different photocatalysts is illustrated by magnetic hysteresis ((M−H)) loops in Fig. 9B. (M−H) loop of the 50% MIL-100/MIL-53 (Fe) photocatalyst at room temperature represents the maximum magnetization value compared to MIL-100 (Fe) and MIL-53 (Fe). However, the magnetization value of the 50% MIL-100/MIL-53 (Fe) photocatalyst is still too small to separate photocatalyst powder by a conventional permanent magnet [2]. The potential magnetic behavior can be expected for MOFs and magnetic materials composite photocatalyst in the further experiments. As shown in Fig. 10A, after four-cycle photocatalytic reactions, the photocatalytic activity of the 50% MIL-100/MIL-53 (Fe) photocatalyst is rarely declined. Fig. 10B presents that the crystal structure of the 50% MIL-100/MIL-53 (Fe) photocatalyst has no significate change before and after the photocatalytic process. Based on the above results, it is demonstrated that the 50% MIL-100/MIL-53 (Fe) photocatalyst shows a good stability and recyclability in the photodegradation of MC-LR.

3.5. Photocatalytic mechanism and the effect of coordinative immobilized layers for the 50% MIL-100/MIL-53 (Fe) photocatalyst

The photocatalytic mechanism for the removal of MC-LR with the 50% MIL-100/MIL-53 (Fe) photocatalyst is illustrated in Fig. 11. Both MIL-100 (Fe) and MIL-53 (Fe) can be excited to yield photogenerated carriers under visible light irradiation. In the 50% MIL-100/MIL-53 (Fe) photocatalyst, the conduction band (CB) of MIL-53 (Fe) and the valence band (VB) of MIL-100 (Fe) will accumulate a large amount of photogenerated electrons (e^-) and holes (h^+) due to the migration of photogenerated carriers. More photogenerated holes as the main active species can be directly involved in the photocatalytic degradation of MC-LR on the surface of MIL-100 (Fe). Therefore, the synergistic effect of the 50% MIL-100/MIL-53 (Fe) photocatalyst, MIL-100 (Fe) as the active sites and MIL-53 (Fe) as the light harvesting support, plays an important role for the removal of MC-LR.

Upon light irradiation, electron excitation takes place in organic linkers, followed electrons transfer on the iron (III) oxide clusters [42]. Therefore, coordinate immobilized layers consisted of iron (III) oxide clusters between MIL-100 (Fe) and MIL-53 (Fe) can be involved into the migration of photogenerated carriers. And then the efficient separation of photogenerated electron-hole pairs is achieved, resulting that more

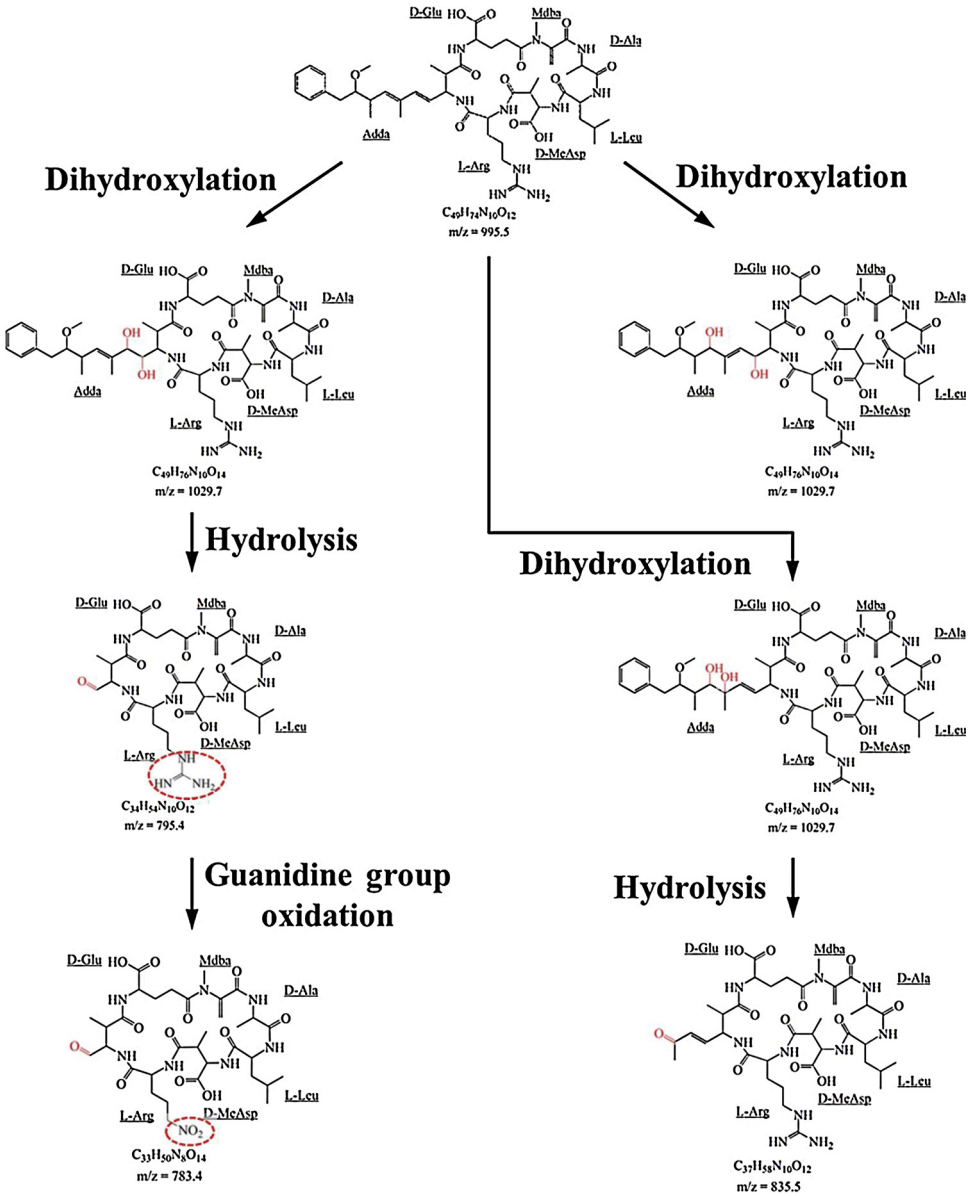

Fig. 8. Proposed degradation intermediates and cleavage pathways of MC-LR with the 50% MIL-100/MIL-53 (Fe) photocatalyst.

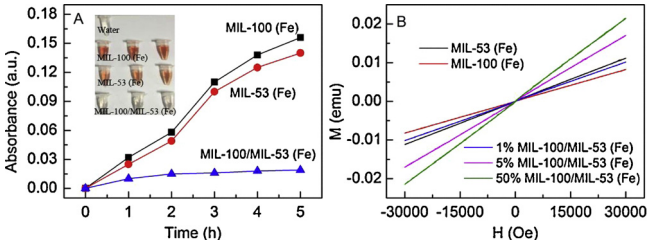

Fig. 9. (A) Fe leaching result of MIL-100 (Fe), MIL-53 (Fe) and the 50% MIL-100/MIL-53 (Fe) photocatalyst (Inset: the photo of the aqueous solution during the photocatalytic process), (B) (M − H) loops of different photocatalysts at room temperature.

photogenerated holes are used to enhance the removal of MC-LR for the MIL-100/MIL-53 (Fe) photocatalyst. Meanwhile, the cycling stability and the Fe^{3+} chelation of the 50% MIL-100/MIL-53 (Fe) photocatalyst are relatively improved with the modification of MIL-100 (Fe) on the surface of MIL-53 (Fe). Based on the above results, the effect of coordinative immobilized layers between MIL-100 (Fe) and MIL-53 (Fe) can be well explained to the stable and efficient photocatalytic activity of the 50% MIL-100/MIL-53 (Fe) photocatalyst for the removal of MC-LR.

4. Conclusions

In summary, the MIL-100/MIL-53 (Fe) photocatalysts were synthesized by the electrostatic interaction between MIL-100 (Fe) and MIL-53 (Fe). Compared to MIL-100 (Fe) and MIL-53 (Fe), the MC-LR photodegradation of the 50% MIL-100/MIL-53 (Fe) photocatalyst achieved 96.5% with the low dosage of 0.02 g/L under visible light irradiation for 3 h due to the pore-effect adsorption and the effective separation of photogenerated carriers. The effect of coordinative immobilized layers between MIL-100 (Fe) and MIL-53 (Fe) contributed to the stable and efficient photocatalytic activity of the 50% MIL-100/MIL-53 (Fe) photocatalyst for the removal of MC-LR. The MC-LR photodegradation mechanism and degradation pathway, which the photogenerated holes (h^+) was directly oxidation to form different intermediate products, were proposed by radical capture experiments and LC-MS analysis in the photocatalytic process. This investigation will further understand

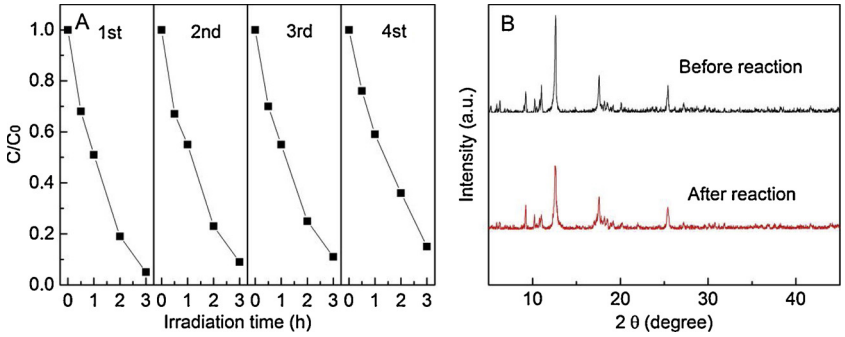

Fig. 10. (A) Cycling tests of the 50% MIL-100/MIL-53 (Fe) photocatalyst in the removal of MC-LR [photocatalyst dosage] = 0.02 g/L, [MC-LR] = 4.5 mg/L, pH = 7 (B) XRD of the 50% MIL-100/MIL-53 (Fe) photocatalyst before and after the photocatalytic process.

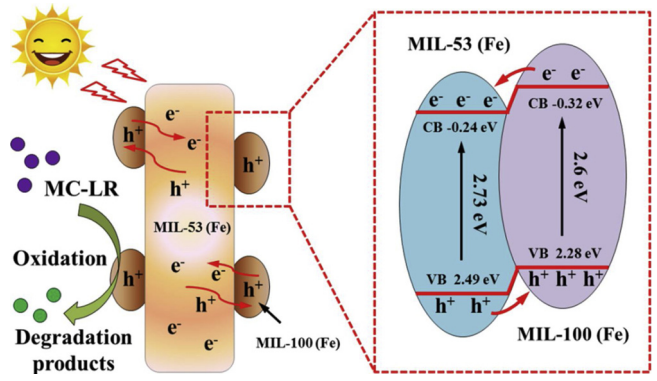

Fig. 11. A schematic illustration of the photocatalytic mechanism for the MC-LR degradation by the 50% MIL-100/MIL-53 (Fe) photocatalyst under visible light irradiation.

the photocatalytic mechanism of MC-LR and inspire the exploration of the stable and efficient MOFs-based photocatalysts.

Acknowledgements

This work was financially supported by National Natural Science Foundation of China (No: 21677086, 21577078, 21577077), Innovation Group Project of Hubei province (No: 2015CFA021), Project funded by China Postdoctoral Science Foundation (2018M640721), Postdoctoral Science Foundation of Hubei province (G83) and open fund of key laboratory of inorganic nonmetallic crystalline and energy conversion materials (China Three Gorges University) (2018KIE05).

Appendix A. Supplementary data

Supplementary material related to this article can be found, in the online version, at doi:https://doi.org/10.1016/j.apcatb.2019.04.086.

References

[1] X. Zhang, J. He, S. Xiao, X. Yang, Elimination kinetics and detoxification mechanisms of microcystin-LR during UV/chlorine process, Chemosphere 214 (2019) 702–709.
[2] C. Han, L. Machala, I. Medrik, R. Prucek, R.P. Kralchevska, D.D. Dionysiou, Degradation of the cyanotoxin microcystin-LR using iron-based photocatalysts under visible light illumination, Environ. Sci. Pollut. Res. 24 (2017) 19435–19443.
[3] WHO, Guidelines for Drinking-water Quality, fourth ed., World Health Organization, Geneva, Switzerland, 2011.
[4] X. Ren, G. Zeng, L. Tang, J. Wang, J. Wan, H. Feng, B. Song, C. Huang, X. Tang, Effect of exogenous carbonaceous materials on the bioavailability of organic pollutants and their ecological risks, Soil Biol. Biochem. 116 (2018) 70–81.
[5] X. Ren, G. Zeng, L. Tang, J. Wang, J. Wan, Y. Liu, J. Yu, H. Yi, S. Ye, R. Deng, Sorption, transport and biodegradation-an insight into bioavailability of persistent organic pollutants in soil, Sci. Total Environ. 610–611 (2018) 1154–1163.
[6] W. Liao, Y. Zhang, M. Zhang, M. Murugananthan, S. Yoshihara, Photoelectrocatalytic degradation of microcystin-LR using Ag/AgCl/TiO_2 nanotube arrays electrode under visible light irradiation, Chem. Eng. J. 231 (2013) 455–463.
[7] Q. Guo, H. Li, Q. Zhang, Y. Zhang, Fabrication, characterization and mechanism of a novel Z-scheme Ag_3PO_4/NG/polyimide composite photocatalyst for microcystin-LR degradation, Appl. Catal. B: Environ. 229 (2018) 192–203.
[8] A.M. Freitas, C. Sirtori, C.A. Lenz, P.G. Peralta Zamora, Microcystin-LR degradation by solar photo-Fenton, UV-A/photo-Fenton and UV-C/H_2O_2: a comparative study, Photochem. Photobiol. Sci. 12 (2013) 696–702.
[9] M.G. Antoniou, I. Boraei, M. Solakidou, Y. Deligiannakis, M. Abhishek, L.A. Lawton, C. Edwards, Enhancing photocatalytic degradation of the cyanotoxin microcystin-LR with the addition of sulfate-radical generating oxidants, J. Hazard. Mater. 360 (2018) 461–470.
[10] S. Chae, T. Noeiaghaei, Y. Oh, I.S. Kim, J.S. Park, Effective removal of emerging dissolved cyanotoxins from water using hybrid photocatalytic composites, Water Res. 149 (2019) 421–431.
[11] N. Khadgi, A.R. Upreti, Photocatalytic degradation of microcystin-LR by visible light active and magnetic, $ZnFe_2O_4$-Ag/rGO nanocomposite and toxicity assessment of the intermediates, Chemosphere 221 (2019) 441–451.
[12] L.B. Li, R.B. Lin, R. Krishna, H. Li, S.C. Xiang, H. Wu, J.P. Li, W. Zhou, B.L. Chen, Ethane/ethylene separation in a metal-organic framework with iron-peroxo sites, Science 362 (2018) 443–446.
[13] Q.H. Yang, Q. Xu, H.L. Jiang, Metal-organic frameworks meet metal nanoparticles: synergistic effect for enhanced catalysis, Chem. Soc. Rev. 46 (2017) 4774–4808.
[14] Z. Yang, X. Xu, X. Liang, C. Lei, Y. Wei, P. He, B. Lv, H. Ma, Z. Lei, MIL-53 (Fe)-graphene nanocomposites: efficient visible-light photocatalysts for the selective oxidation of alcohols, Appl. Catal. B: Environ. 198 (2016) 112–123.
[15] K.G.M. Laurier, F. Vermoortele, R. Ameloot, D.E. De Vos, J. Hofkens, M.B.J. Roeffaers, Iron (III)-based metal-organic frameworks as visible light photocatalysts, J. Am. Chem. Soc. 135 (2013) 14488–14491.
[16] D. Wang, F. Jia, H. Wang, F. Chen, Y. Fang, W. Dong, G. Zeng, X. Li, Q. Yang, X. Yuan, Simultaneously efficient adsorption and photocatalytic degradation of tetracycline by Fe-based MOFs, J. Colloid Interface Sci. 519 (2018) 273–284.
[17] P.L. Llewellyn, P. Horcajada, G. Maurin, T. Devic, N. Rosenbach, S. Bourrelly, C. Serre, D. Vincent, S. Loera-Serna, Y. Filinchuk, G. Férey, Complex adsorption of short linear alkanes in the flexible metal-organic framework MIL-53 (Fe), J. Am. Chem. Soc. 131 (2009) 13002–13008.
[18] R. Liang, F. Jing, L. Shen, N. Qin, L. Wu, MIL-53 (Fe) as a highly efficient bifunctional photocatalyst for the simultaneous reduction of Cr(VI) and oxidation of dyes, J. Hazard. Mater. 287 (2015) 364–372.
[19] Y. Gao, S. Li, Y. Li, L. Yao, Zhang H, Accelerated photocatalytic degradation of organic pollutant over metal-organic framework MIL-53 (Fe) under visible LED light mediated by persulfate, Appl. Catal. B: Environ. 202 (2017) 165–174.
[20] T. Araya, M. Jia, J. Yang, P. Zhao, K. Cai, W. Ma, Y. Huang, Resin modified MIL-53 (Fe) MOF for improvement of photocatalytic performance, Appl. Catal. B: Environ. 203 (2017) 768–777.
[21] X. Li, Y. Pi, Q. Hou, H. Yu, Z. Li, Y. Li, J. Xiao, Amorphous TiO_2@NH_2-MIL-125 (Ti) homologous MOF-encapsulated heterostructures with enhanced photocatalytic activity, Chem. Commun. 54 (2018) 1917–1920.
[22] P. Karthik, R. Vinoth, P. Zhang, W. Choi, E. Balaraman, B. Neppolian, π-π interaction between metal-organic framework and reduced graphene oxide for visible-light photocatalytic H_2 production, ACS Appl. Energy Mater. 1 (2018) 1913–1923.
[23] L. Liu, L. Zhang, F. Wang, K. Qi, H. Zhang, X. Cui, W. Zheng, Bi-metal-organic frameworks type II heterostructures for enhanced photocatalytic styrene oxidation, Nanoscale 11 (2019) 7554–7559, https://doi.org/10.1039/C9NR00790C.
[24] S. Abdpour, E. Kowsari, M.R.A. Moghaddam, Synthesis of MIL-100 (Fe)@MIL-53 (Fe) as a novel hybrid photocatalyst and evaluation photocatalytic and photoelectrochemical performance under visible light irradiation, J. Solid State Chem. 262 (2018) 172–180.
[25] W. Xia, X. Zhang, L. Xu, Y. Wang, J. Lin, R. Zou, Facile and economical synthesis of metal-organic framework MIL-100 (Al) gels for high efficiency removal of microcystin-LR, RSC Adv. 3 (2013) 11007–11013.
[26] Y. Wei, Y. Xia, Pyridine-grafted Cr-based metal-organic frameworks for adsorption and removal of microcystin-LR from aqueous solution, Environ. Sci. Water Res. Technol. 5 (2019) 577–584.
[27] S.H. Huo, X.P. Yan, Metal-organic framework MIL-100 (Fe) for the adsorption of malachite green from aqueous solution, J. Mater. Chem. 22 (2012) 7449–7455.
[28] L. Ai, L. Li, C. Zhang, Fu J, J. Jiang, MIL-53 (Fe): a metal-organic framework with

intrinsic peroxidase-like catalytic activity for colorimetric biosensing, Chem. Eur. J. 19 (2013) 15105–15108.
[29] H.L. Tian, H.Q. Fan, J.W. Ma, Z.Y. Liu, L.T. Ma, S.H. Lei, J.W. Fang, C.B. Long, Pt-decorated zinc oxide nanorod arrays with graphitic carbon nitride nanosheets for highly efficient dual-functional gas sensing, J. Hazard. Mater. 341 (2018) 102–111.
[30] R. Liang, L. Shen, F. Jing, N. Qin, L. Wu, Preparation of MIL-53 (Fe)-reduced graphene oxide nanocomposites by a simple self-assembly strategy for increasing interfacial contact: efficient visible-light photocatalysts, ACS Appl. Mater. Interfaces 7 (2015) 9507–9515.
[31] M. Tong, D. Liu, Q. Yang, S. Devautour-Vinot, G. Maurin, C. Zhong, Influence of framework metal ions on the dye capture behavior of MIL-100 (Fe, Cr) MOF type solids, J. Mater. Chem. A 1 (2013) 8534–8537.
[32] C.H. Hendon, D. Tiana, M. Fontecave, C. Sanchez, L. D'arras, C. Sassoye, L. Rozes, C. Mellot-Draznieks, A. Walsh, Engineering the optical response of the titanium-MIL-125 metal-organic framework through ligand functionalization, J. Am. Chem. Soc. 135 (2013) 10942–10945.
[33] C.X. Yang, H.B. Ren, X.P. Yan, Fluorescent metal-organic framework MIL-53 (Al) for highly selective and sensitive detection of Fe^{3+} in aqueous solution, Anal. Chem. 85 (2013) 7441–7446.
[34] J.A. Park, S.M. Jung, I.G. Yi, J.W. Choi, S.B. Kim, S.H. Lee, Adsorption of microcystin-LR on mesoporous carbons and its potential use in drinking water source, Chemosphere 177 (2017) 15–23.
[35] S. Kato, K. Otake, H. Chen, I. Akpinar, C.T. Buru, T. Islamoglu, R.Q. Snurr, O.K. Farha, Zirconium-based metal-organic frameworks for the removal of protein-bound uremic toxin from human serum albumin, J. Am. Chem. Soc. 141 (2019) 2568–2576.
[36] M. Pelaez, B. Baruwati, R.S. Varma, R. Luque, D.D. Dionysiou, Microcystin-LR removal from aqueous solutions using a magnetically separable N-doped TiO_2 nanocomposite under visible light irradiation, Chem. Commun. 49 (2013) 10118–10120.
[37] Y. Fang, Y. Huang, J. Yang, P. Wang, G. Cheng, Unique ability of BiOBr to decarboxylate D-Glu and D-MeAsp in the photocatalytic degradation of microcystin-LR in water, Environ. Sci. Technol. 45 (2011) 1593–1600.
[38] Y. Xue, P. Wang, C. Wang, Y. Ao, Efficient degradation of atrazine by BiOBr/UiO-66 composite photocatalyst under visible light irradiation: environmental factors, mechanisms and degradation pathways, Chemosphere 203 (2018) 497–505.
[39] S. Wang, L. Wang, W. Ma, D.M. Johnson, Y. Fang, M. Jia, Y. Huang, Moderate valence band of bismuth oxyhalides (BiOXs, X = Cl, Br, I) for the best photocatalytic degradation efficiency of MC-LR, Chem. Eng. J. 259 (2015) 410–416.
[40] A. Islam, D. Jeon, J. Ra, J. Shin, T.Y. Kim, Y. Lee, Transformation of microcystin-LR and olefinic compounds by ferrate (VI): oxidative cleavage of olefinic double bonds as the primary reaction pathway, Water Res. 141 (2018) 268–278.
[41] X. Feng, H. Chen, F. Jiang, In-situ ethylenediamine-assisted synthesis of a magnetic iron-based metal-organic framework MIL-53 (Fe) for visible light photocatalysis, J. Colloid Interface Sci. 494 (2017) 32–37.
[42] J.J. Du, Y.P. Yuan, J.X. Sun, F.M. Peng, X. Jiang, L.G. Qiu, A.J. Xie, Y.H. Shen, J.F. Zhu, New photocatalysts based on MIL-53 metal-organic frameworks for the decolorization of methylene blue dye, J. Hazard. Mater. 190 (2011) 945–951.